

Joint Sparse Graph for Enhanced MIMO-AFDM Receiver Design

Qu Luo, *Member, IEEE*, Jing Zhu, *Member, IEEE*, Zilong Liu, *Senior Member, IEEE*, Yanqun Tang, Pei Xiao, *Senior Member, IEEE*, Gaojie Chen, *Senior Member, IEEE*, and Jia Shi, *Member, IEEE*.

Abstract—Affine frequency division multiplexing (AFDM) is a promising chirp-assisted multicarrier waveform for future high-mobility communications. This paper is devoted to enhanced receiver design for multiple-input–multiple-output AFDM (MIMO-AFDM) systems. Firstly, we introduce a unified variational inference (VI) approach to approximate the target posterior distribution, under which the belief propagation (BP) and expectation propagation (EP)-based algorithms are derived. As both VI-based detection and low-density parity-check (LDPC) decoding can be expressed by bipartite graphs in MIMO-AFDM systems, we construct a joint sparse graph (JSG) by merging the graphs of these two for low-complexity receiver design. Then, based on this graph model, we present the detailed message propagation of the proposed JSG. Additionally, we propose an enhanced JSG (E-JSG) receiver based on the linear constellation encoding model. The proposed E-JSG eliminates the need for interleavers, de-interleavers, and log-likelihood ratio transformations, thus leading to concurrent detection and decoding over the integrated sparse graph. To further reduce detection complexity, we introduce a sparse channel method by approximating multiple graph edges with insignificant channel coefficients into a single edge on the VI graph. Simulation results show the superiority of the proposed receivers in terms of computational complexity, detection and decoding latency, and error rate performance compared to the conventional ones.

Index Terms—Affine frequency division multiplexing (AFDM), multiple-input–multiple-output AFDM (MIMO-AFDM), variational inference (VI), joint sparse graph, low complexity detection and decoding.

I. INTRODUCTION

A. Background

NEXT generation wireless systems and standards e.g., beyond 5G, 6G are envisioned to provide a wide range of data services, including ultra-reliable, high-rate, and low-latency communications in highly dynamic environments, such as vehicle-to-everything, unmanned aerial vehicles, high-speed trains, and low-earth-orbit satellite systems, etc. [1], [2]. In these scenarios, one often needs to deal with the rapidly time-varying channels [3], [4]. The legacy multicarrier systems primarily rely on orthogonal frequency division multiplexing (OFDM), thanks to its advantages (e.g., efficient hardware implementation, capability of intersymbol interference mitigation) in linear time-invariant channels [5]. Nevertheless,

OFDM is sensitive to carrier frequency offsets and Doppler shifts/spreads in rapidly time-varying channels and hence may suffer from drastically degraded error performances [3].

Extensive efforts have been dedicated to designing novel modulation waveforms to support reliable communications in high mobility channels. For example, orthogonal time–frequency space (OTFS) modulation [3], [6] and orthogonal chirp division multiplexing (OCDM) [7], [8] have attracted substantial research attention. The former modulates the information symbols in the delay-Doppler domain instead of the conventional time–frequency domain. By doing so, one can effectively convert a time-variant channel into a two-dimensional (2D) quasi-static channel in delay-Doppler domain [3], [6], [9]. In contrast, OCDM, building upon the discrete Fresnel transform (DFnT), modulates the information symbols using a class of orthogonal chirp subcarriers (SCs) [7]. Both OTFS and OCDM have demonstrated superior error performances over OFDM [10], [11]. However, the 2D structure of OTFS requires radical change of the transceivers (compared to that of OFDM), whilst it suffers from large overhead for sending pilots and multiuser signals [11]. OCDM, on the other hand, may not be able to achieve optimal performance when its chirp rate does not fit the specific delay-Doppler profile of the channel [11].

Recently, Affine frequency division multiplexing (AFDM) is another appealing solution for efficient and reliable communications over high-mobility channels [11]. Similar to OCDM, information symbols in AFDM are multiplexed on a number of orthogonal chirp SCs through the discrete affine Fourier transform (DAFT) [12]. By appropriately adjusting the chirp rate based on the delay-Doppler profile of the channel, AFDM enables a separable and quasi-static channel representation, thereby achieving full diversity over doubly selective channels [11]. Since the DAFT employed in AFDM is a generalization of many other transforms, such as the discrete Fourier transform (DFT) and DFnT, AFDM generalizes OFDM and OCDM as special cases. More importantly, AFDM enjoys a high compatibility to the legacy OFDM as DAFT can be efficiently implemented through fast Fourier transform (FFT) with additional two one-tap filters [13]. These advantages make AFDM as a promising candidate multicarrier waveform for the next generation wireless systems [14], [15].

B. Related Works

AFDM has attracted a plethora of research attempts from various aspects, such as system impairments [13], [16], channel estimation [17], [18], signal detection [19], [20], and inter-

Qu Luo, Jing Zhu, Pei Xiao and Gaojie Chen are with the 5G & 6G Innovation Centre, University of Surrey, U. K. (email: {q.u.luo, j.zhu, p.xiao, gaojie.chen }@surrey.ac.uk). Zilong Liu is with the School of Computer Science and Electronics Engineering, University of Essex, U. K. (email: zilong.liu@essex.ac.uk). Yanqun Tang is with the School of Electronics and Communication Engineering, Sun Yat-sen University, China (email: tangyq8@mail.sysu.edu.cn). Jia Shi is with the School of Telecommunications Engineering, Xidian University, Xi'an, China (email: jiashi@xidian.edu.cn).

grated sensing and communications [21]–[23]. The authors in [13] evaluated the performance of AFDM over high-mobility scenarios and in high-frequency bands. It is shown that AFDM is robust to the impairments such as carrier frequency offset and phase noise. The time and frequency offset estimations for AFDM synchronization have been studied in [16]. In [17], both single pilot and multiple pilots aided channel estimation schemes for AFDM were considered. In [18], an embedded pilot-aided channel estimation scheme for AFDM with multiple input and multiple output (MIMO), called MIMO-AFDM, was investigated. Moreover, a low complexity iterative decision feedback equalizer based on weighted maximal ratio combining scheme was introduced in [19] for efficient symbol detection by exploiting the channel sparsity in AFDM. A generalized message passing algorithm (MPA)-based detection scheme was developed in [20]. However, the complexity of the MPA detector grows exponentially as the number of multipaths increases. By fully exploiting its inherent chirp nature of AFDM, it has also been applied for integrated sensing and communications (ISAC). In particular, a low complexity algorithm based on matched filtering was developed in [21] for estimating high resolution target range with the AFDM waveform. In [22], an AFDM-based ISAC system was introduced, which utilizes a time-domain parameter estimation scheme. Very recently, [23] proposed an AFDM-based ISAC system using only chirp subcarrier. It shows that sensing with one chirp subcarrier allows simple self-interference cancellation, thus avoiding the need for expensive full duplex methods.

AFDM has also been integrated with code-domain non-orthogonal multiple access or modulation to achieve higher spectrum efficiency and enhanced reliability [24]–[26]. Specifically, [24] and [27] studied the AFDM-empowered sparse code multiple access (SCMA) for massive connectivity over high mobility communications. In comparison to OFDM-SCMA, AFDM-SCMA exhibits significantly improved error performance. In addition, [25], [26] proposed index modulation (IM)-empowered AFDM systems, which was shown to outperform its OFDM-IM counterpart.

C. Motivations and Contributions

The aforementioned works have shown the advantages of AFDM in high-mobility communications due to its ability to achieve *full diversity* [11], [13], [24]–[26]. However, the *full diversity* can only be attained with a sophisticated receiver that implements the optimal maximum *a posteriori* (MAP) detection [28], such as MPA and sphere decoder. In addition, it should be noted that existing works on AFDM generally focused on uncoded systems and little has been reported on the coded AFDM system performances. Recently, [8] compared the uncoded and coded BER performances of OCDM and OFDM by employing a minimum mean square error (MMSE) detector and a rate-1/3 convolutional code. It was shown in [8] that OCDM achieves better uncoded BER performance but similar coded BER performance compared to OFDM. This is reasonable due to the frequency diversity attained by coded OFDM. The above observations can be readily extended to AFDM systems due to its generic chirp nature. This also implies that enhanced detection and decoding in AFDM should

be carefully designed by considering its inherent features for fully exploiting the diversity gain. In addition, while there is extensive literature on efficient iterative receiver design, such as the Turbo iterative structure [29], [30] and orthogonal approximate message passing design [24], [31], developing more advanced and low-complexity AFDM receiver remains largely unexplored.

On the other hand, the amalgamation of MIMO and AFDM, i.e., MIMO-AFDM, can be leveraged to achieve higher spectrum efficiency and lower error rate. Although the channel estimation of MIMO-AFDM was studied in [17], the efficient receiver design in MIMO-AFDM is a largely open research topic.

Against the above background and research gaps, this paper aims to develop novel low-complexity joint detection and decoding schemes fully exploiting the system diversity in MIMO-AFDM systems. Specifically, we formulate the MIMO-AFDM detection as a Bayesian inference problem for computing the marginal posterior distribution [32]. We advocate the use of variational inference (VI) [33] as an approximate inference algorithm in probabilistic models. The principle of VI is to approximate the target posterior distribution using a simple distribution, thereby transforming an intractable inference problem into a tractable one [34], [35]. Our second key innovation is to represent the joint distribution of the transmitted and received signal in MIMO-AFDM as a sparse factor graph, referred to as the VI graph. By adopting low-density parity check (LDPC) codes as the channel code [36], we merge the VI graph and the relevant LDPC factor graph into a joint sparse graph (JSG).

The main contributions of this paper are summarized as follows:

- We formulate MIMO-AFDM detection as a Bayesian inference problem for computing the marginal posterior distribution. Specifically, we introduce a unified VI approach to approximate the target posterior distribution, upon which the belief propagation (BP) and expectation propagation (EP)-based algorithms can be derived. Subsequently, both BP-JSG and EP-JSG are employed for highly efficient message propagation.
- Inspired by the linear constellation encoding model, we introduce an enhanced JSG (E-JSG) to eliminate the use of interleavers, de-interleavers, symbol-to-bit, and bit-to-symbol log-likelihood ratio (LLR) transformations. As such, one can merge the detection and decoding for E-JSG by efficiently passing the belief messages over the integrated sparse graph. In addition, for reduced receiver processing, we propose a sparse channel method. The main idea of this approach is to approximate multiple graph edges with insignificant channel coefficients into a single edge on the VI graph.
- We present extensive numerical results to demonstrate the superiority of the proposed JSG receivers in terms of lower computational complexity and reduced detection and decoding latency compared to conventional MMSE and turbo-like receivers. Furthermore, the proposed JSG receivers can exploit multipath diversity and Doppler diversity in MIMO-AFDM systems more efficiently, giving

rise to improved coded BER performance compared to conventional receivers.

D. Organization

This paper is organized as follows: Section II describes the system model of MIMO-AFDM. The proposed VI-JSG is presented in Section III, covering the principles of VI, joint factor representation of MIMO-AFDM, and the message passing in VI-JSG. Section IV introduces the proposed enhanced VI-JSG and the complexity reduction in the JSG. The simulation results are presented and discussed in Section V. Section VI concludes the paper.

E. Notation

The n -dimensional complex, real and binary vector spaces are denoted as \mathbb{C}^n , \mathbb{R}^n and \mathbb{B}^n , respectively. Similarly, $\mathbb{C}^{k \times n}$, $\mathbb{R}^{k \times n}$ and $\mathbb{B}^{k \times n}$ denote the $(k \times n)$ -dimensional complex, real and binary matrix spaces, respectively. $\mathcal{CN}(0, 1)$ denotes the complex Gaussian distribution with zero-mean and unit-variance. \mathbf{I}_n denotes an $n \times n$ -dimensional identity matrix. $\text{diag}(\mathbf{x})$ gives a diagonal matrix with the diagonal vector of \mathbf{x} . $(\cdot)^T$ and $(\cdot)^H$ denote the transpose and the Hermitian transpose operation, respectively.

II. MIMO-AFDM COMMUNICATION MODEL

This section introduces the MIMO-AFDM signal model. Specifically, we start by introducing the AFDM modulation, channel, demodulation and input-output (I/O) relation in the single-input and single-output AFDM (SISO-AFDM) system, which is shown in Fig. 1. Subsequently, we extend the SISO-AFDM to the MIMO-AFDM case.

A. SISO-AFDM Communication Model

This section presents the signal model of a SISO-AFDM system, as shown in Fig. 1.

1) *AFDM modulation*: Denoted $\mathbf{x}_{\text{SISO}} \in \mathbb{C}^{N \times 1}$ by the transmitted vector in the DAFT domain. Then the modulated symbol is obtained by taking the IDAFT of \mathbf{x}_{SISO} , i.e.,

$$s_n = \sum_{m=0}^{N-1} x_m \varphi_n(m), n = 0, 1, \dots, N-1, \quad (1)$$

where $\varphi_n(m)$ is the AFT kernel at the m th SC and associated to the n th modulated symbol. The AFT kernel of Type-A in [11] is considered, i.e., $\varphi_n(m) = \frac{1}{\sqrt{N}} e^{j2\pi(c_1 n^2 + c_2 m^2 + \frac{nm}{N})}$, where $c_1 \geq 0$ and $c_2 \geq 0$ are the AFDM parameters. Note that (1) can be written in the matrix form as $\mathbf{s} = \Lambda_{c_1}^H \mathbf{F}^H \Lambda_{c_2}^H \mathbf{x}_{\text{SISO}} \equiv \mathbf{A}^H \mathbf{x}_{\text{SISO}}$, where $\mathbf{A} \equiv \Lambda_{c_2} \mathbf{F} \Lambda_{c_1}$ is the DAFT matrix, $\Lambda_c = \text{diag}(e^{-j2\pi c n^2}, n = 0, 1, \dots, N-1)$, \mathbf{F} is the DFT matrix with its element at the m th column and the n th row given by $e^{-j2\pi mn/N} / \sqrt{N}$.

Then, a chirp-periodic prefix (CPP) is applied to the transmitted signal [11]. The CCP with length N_{CPP} is given by

$$s_n = s_{N+n} e^{-j2\pi c_1 (N^2 + 2Nn)}, n = -N_{\text{CPP}}, \dots, -1. \quad (2)$$

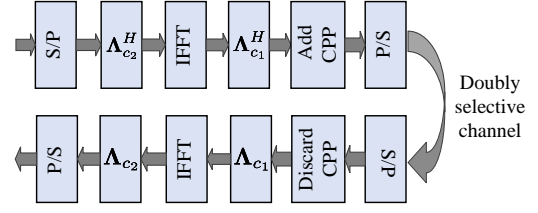


Fig. 1: Example of SISO-AFDM communication model.

2) *Channel*: We consider a doubly selective channel with the channel response at time n and delay d given by

$$g_{n,d} = \sum_{p=1}^P h_p e^{-j \frac{2\pi}{N} \nu_p n} \delta(d - d_p), \quad (3)$$

where $\delta(\cdot)$ denotes the Dirac delta function, P is the number of paths, and h_p , ν_p and d_p are the channel gain, Doppler shift and the integer delay of the p th path, respectively. Note that ν_p is normalized with respect to the SC spacing and can be expressed as $\nu_p = \alpha_p + \beta_p$, where $\alpha_p \in [-\alpha_{\text{max}}, \alpha_{\text{max}}]$ and $\beta_p \in (-\frac{1}{2}, \frac{1}{2}]$ denote the integer and fractional parts of ν_i , respectively, and α_{max} is the maximum integer Doppler.

3) *AFDM demodulation*: The received signal in the time domain after discarding the CPP can be expressed as

$$\tilde{r}_n = \sum_{d=0}^{\infty} s_{n-d} g_{n,d} + \tilde{w}_n, \quad (4)$$

where $w_n \sim \mathcal{CN}(0, N_0)$ is the additive Gaussian noise. After discarding the CPP, (4) can be re-written in the matrix form as $\tilde{\mathbf{r}} = \sum_{p=1}^P \tilde{\mathbf{H}}_p \mathbf{s} + \tilde{\mathbf{w}}$, where $\tilde{\mathbf{w}}$ is the noise vector in the time domain, $\tilde{\mathbf{H}}_p = h_p \mathbf{\Gamma}_{\text{CPP}_p} \mathbf{\Delta}_{\nu_p} \mathbf{\Pi}^{d_p}$ is the time domain channel matrix of the p th path, $\mathbf{\Delta}_{\nu_p} = \text{diag}(e^{-j \frac{2\pi}{N} \nu_p n}, n = 0, 1, \dots, N-1)$ models the Doppler effect, $\mathbf{\Pi} = \begin{bmatrix} 0 & \dots & 0 & 1 \\ 1 & \dots & 0 & 0 \\ \vdots & \ddots & \ddots & \vdots \\ 0 & \dots & 1 & 0 \end{bmatrix}_{N \times N}$

denotes the forward cyclic-shift matrix, and $\mathbf{\Gamma}_{\text{CPP}_p} = \text{diag}\left(\begin{cases} e^{-j2\pi c_1 (N^2 - 2N(d_p - n))}, & n < d_p, \\ 1, & n \geq d_p, \end{cases}\right)$ denotes the effective CCP matrix.

Finally, the received signal in the DAFT domain is obtained by applying the DAFT transform, i.e.,

$$\mathbf{r} = \Lambda_{c_2} \mathbf{F} \Lambda_{c_1} \tilde{\mathbf{r}} \equiv \mathbf{A} \tilde{\mathbf{r}}. \quad (5)$$

4) *The I/O relation*: Substituting (1), (3) and (4) into (5), yields the I/O relation in the time domain as

$$r_n = \frac{1}{N} \sum_{m=0}^{N-1} \sum_{p=1}^P h_p \eta(d_p, n, m) \gamma(d_p, \nu_p, n, m) x_m + w_n, \quad (6)$$

where

$$\eta(d_p, n, m) = e^{j \frac{2\pi}{N} (N c_1 d_p^2 - m d_p + N c_2 (m^2 - n^2))}, \quad (7a)$$

$$\gamma(d_p, \nu_p, n, m) = \frac{e^{-j2\pi(n-m+\text{Ind}_p+\beta_p)} - 1}{e^{-j \frac{2\pi}{N} (n-m+\text{Ind}_p+\beta_p)} - 1}, \quad (7b)$$

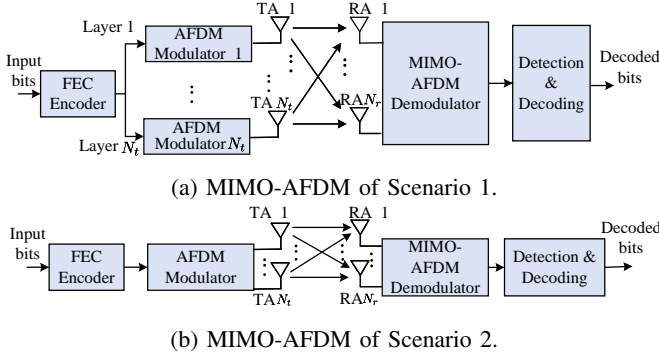


Fig. 2: System model of MIMO-AFDM.

and $\text{Ind}_p = (\alpha_p + 2Nc_1d_p)_N$. Note that the I/O relation in the DAFT domain can also be written in the matrix form, i.e.,

$$\mathbf{r} = \sum_{p=1}^P h_p \underbrace{\Lambda_{c_2} \mathbf{F} \Lambda_{c_1} \Gamma \mathbf{C} \mathbf{P} \mathbf{P}^H \Delta_{f_p} \Pi^{d_p} \Lambda_{c_1}^H \mathbf{F}^H \Lambda_{c_2}^H}_{\bar{\mathbf{H}}_p} \mathbf{x}_{\text{SISO}} + \mathbf{w}_{\text{SISO}} = \mathbf{H}_{\text{SISO}} \mathbf{x}_{\text{SISO}} + \mathbf{w}_{\text{SISO}}, \quad (8)$$

where $\mathbf{H}_{\text{SISO}} = \sum_{p=1}^P h_p \bar{\mathbf{H}}_p$ is the effective channel matrix and \mathbf{w}_{SISO} is the noise vector with the same distribution of $\tilde{\mathbf{w}}$. It can be shown that the element of $\bar{\mathbf{H}}_p$ at the n th row and the m th column is

$$\bar{\mathbf{H}}_p[n, m] = \eta(d_p, n, m) \gamma(d_p, \nu_p, n, m). \quad (9)$$

In AFDM systems, the parameters c_1 and c_2 can be adjusted so that the non-zero elements of matrix $\bar{\mathbf{H}}_p$ in each path do not overlap within \mathbf{H}_{SISO} , resulting in a comprehensive delay-Doppler channel representation.

B. Frameworks of MIMO-AFDM Schemes

We consider a MIMO system where the transmitter is equipped with N_t transmit antennas (TAs) and the BS is equipped with N_r receive antennas (RAs). Denoted $\mathbf{H}^{(r,t)} \in \mathbb{C}^{N \times N}$ by the effective channel matrix from the t th TA to the r th RA. Then the received signal at the r th RA can be expressed as

$$\mathbf{y}_r = \sum_{t=1}^{N_t} \mathbf{H}^{(r,t)} \mathbf{x}_t + \mathbf{w}_r, \quad (10)$$

where $\mathbf{x}_t \in \mathbb{C}^{N \times 1}$ denotes the transmitted data at the t th TA and $\mathbf{w}_r \in \mathbb{C}^{N \times 1}$ denotes the noise vector with $\mathcal{CN}(0, N_0)$ entries. By stacking the received signal of N_r RAs, we have

$$\mathbf{y} = \mathbf{H} \mathbf{x} + \mathbf{w}, \quad (11)$$

where $\mathbf{y} \equiv [\mathbf{y}_1^T, \mathbf{y}_2^T, \dots, \mathbf{y}_{N_r}^T]^T \in \mathbb{C}^{N N_r \times 1}$, $\mathbf{x} \equiv [\mathbf{x}_1^T, \mathbf{x}_2^T, \dots, \mathbf{x}_{N_t}^T]^T \in \mathbb{C}^{N N_t \times 1}$, $\mathbf{w} \equiv [\mathbf{w}_1^T, \mathbf{w}_2^T, \dots, \mathbf{w}_{N_r}^T]^T \in \mathbb{C}^{N N_r \times 1}$, and

$$\mathbf{H} \equiv \begin{bmatrix} \mathbf{H}^{(1,1)} & \mathbf{H}^{(1,2)} & \dots & \mathbf{H}^{(1,N_t)} \\ \mathbf{H}^{(2,1)} & \mathbf{H}^{(2,2)} & \dots & \mathbf{H}^{(2,N_t)} \\ \vdots & \vdots & \ddots & \vdots \\ \mathbf{H}^{(N_r,1)} & \mathbf{H}^{(N_r,2)} & \dots & \mathbf{H}^{(N_r,N_t)} \end{bmatrix} \in \mathbb{C}^{N N_r \times N N_t}. \quad (12)$$

Considering the relationship between signals transmitted on different TAs and resource utilization strategies, the MIMO-AFDM frameworks can be categorized into the following two scenarios with the signal mode shown in Fig. 2.

1) Scenario 1 (Multiplexing): As shown in 2(a), the coded bits are split into N_t streams. the n_t th stream is then modulated before transmission over the n_t th antenna.

2) Scenario 2 (Diversity): As shown in 2(b), the coded bits are directly modulated with an AFDM modulator. All the N_t TAs transmit the same modulated signal for diversity enhancement.

III. VARIATIONAL INFERENCE AND GRAPHICAL MODEL

In this section, we first present the VI framework [33] and the proposed JSG representation in MIMO-AFDM. Then, we detail the message propagation process over the JSG based on VI principles.

A. Variational Inference

Given the received observation \mathbf{y} , the goal is to infer the transmitted signal \mathbf{x} . The optimum detection is MAP, which is given by

$$\hat{\mathbf{x}} = \underset{x_m \in \mathcal{X}, \forall m}{\text{argmax}} p(\mathbf{x} | \mathbf{y}), \quad (13)$$

where \mathcal{X} denotes the constellation alphabet. Solving (13) requires a computational complexity order of $|\mathcal{X}|^{N N_t}$ and $|\mathcal{X}|^N$ for Scenarios 1 and 2, respectively, which increases exponentially with N or N_t . The joint probability of the transmitted vector \mathbf{x} and received signal \mathbf{y} can be expressed as: $p(\mathbf{x}, \mathbf{y}) = p(\mathbf{x}) p(\mathbf{y} | \mathbf{x})$, where $p(\mathbf{x})$ denotes the prior probability of \mathbf{x} and $p(\mathbf{y} | \mathbf{x})$ is the likelihood probability. From Bayes' rule, the *a posteriori* probability of \mathbf{x} is given by [33]

$$p(\mathbf{x} | \mathbf{y}) = \frac{p(\mathbf{x}) p(\mathbf{y} | \mathbf{x})}{p(\mathbf{y})} \propto p(\mathbf{x}) p(\mathbf{y} | \mathbf{x}). \quad (14)$$

The marginal posterior probability is calculated as $p(x_m | \mathbf{y}) = \sum_{\sim x_m} p(\mathbf{x} | \mathbf{y})$ which serves as the soft information output for the channel decoder, where $\sum_{\sim x_m}$ denotes the summation over all the arguments except x_m . Unfortunately, the direct calculation of $p(x_m | \mathbf{y})$ incurs high computational complexity. As an approximation approach, the VI technique can be employed for efficient compute (14). The core idea of VI is to find a distribution $q(\mathbf{x} | \mathbf{y})$ from a tractable distribution family \mathcal{Q} , serving as an optimized approximation of the target posterior distribution $p(\mathbf{x} | \mathbf{y})$. As such, the inference problem in (14) can be transformed to a tractable optimization problem. The widely used optimization metrics in VI are the exclusive Kullback-Leibler (KL) divergence $\text{KL}(p|q)$ and inclusive KL divergence $\text{KL}(q|p)$, which measure the similarity between two distributions. The $\text{KL}(p|q)$ and $\text{KL}(q|p)$ are respectively defined as [33]

$$\begin{aligned} \text{KL}(q|p) &= \sum_{\mathbf{x}} q(\mathbf{x} | \mathbf{y}) \log \frac{q(\mathbf{x} | \mathbf{y})}{p(\mathbf{x} | \mathbf{y})}, \\ \text{KL}(p|q) &= \sum_{\mathbf{x}} p(\mathbf{x} | \mathbf{y}) \log \frac{p(\mathbf{x} | \mathbf{y})}{q(\mathbf{x} | \mathbf{y})}. \end{aligned} \quad (15)$$

Note that the KL divergence is non-negative. Moreover, it is neither symmetric nor a distance metric, i.e., $\text{KL}(p|q) \neq \text{KL}(q|p)$. $\text{KL}(q|p)$ divergence emphasizes assignment of low probability mass of q to the location where p is very small. In other words, $\text{KL}(q|p)$ has the propriety of “mode-seeking”

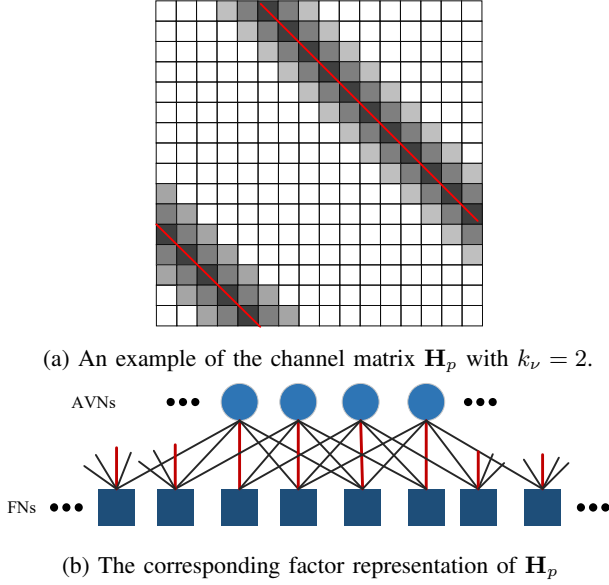


Fig. 3: An example of a channel matrix and its corresponding factor graph representation.

or “zero-forcing” as it forces q to concentrate on one of the local maximum values of p . Conversely, $\text{KL}(p|q)$ divergence emphasizes assignment of high probability mass of q to the location where p has positive mass. Namely, $\text{KL}(p|q)$ metric has the property of mean-seeking or mass covering, meaning that q tends to fit the mean value of p .

In a nutshell, the VI framework provides a unified structure to design detection algorithms by taking $\text{KL}(q|p)$ and $\text{KL}(p|q)$ into consideration. In addition, the VI framework can also be described by using a powerful probabilistic graphical model known as a factor graph. This graphical representation is the key for low-complexity algorithm design, which will be discussed in the sequel.

B. Joint Factor Representation in MIMO-AFDM

Recall (9), for each path, $\eta(d_p, n, m)$ has unit energy, and one has [11]

$$\begin{aligned} |\bar{\mathbf{H}}_p[n, m]| &= \left| \frac{1}{N} \gamma(d_p, \nu_p, n, m) \right| = \left| \frac{\sin(N\theta)}{N \sin(\theta)} \right| \\ &\stackrel{(i)}{\leq} \frac{N-1}{N} |\cos(\theta)| + \frac{1}{N}, \end{aligned} \quad (16)$$

where $\theta \triangleq \frac{\pi}{N}(n - m + \text{Ind}_p + \beta_p)$, $\bar{\mathbf{H}}_p[n, m]$ denotes the entry at the n th row and m th column of $\bar{\mathbf{H}}_p$, and the detailed derivation of (i) is given by the Equations (35) and (36) of [11]. The above bounds hold tight as N increases. It is noted that $\gamma(d_p, \nu_p, n, m)$ achieves the peak energy at $m = (n + \text{Ind}_p)_N$, and the elements in $\bar{\mathbf{H}}_p[n, m]$ become insignificant as m moves away from $(n + \text{Ind}_p)_N$. To better present the message passing over the VI graph, we first assume that those insignificant elements in $\bar{\mathbf{H}}_p[n, m]$ are zeros when m falls outside of $[n + \text{Ind}_p - \nu_v, n + \text{Ind}_p + \nu_v]$. Namely,

$$\bar{\mathbf{H}}_p[n, m] = \begin{cases} \bar{\mathbf{H}}_p[n, m], & (n + \text{Ind}_p - k_\nu)_N \leq m \leq (n + \text{Ind}_p + k_\nu)_N \\ 0, & \text{otherwise} \end{cases}. \quad (17)$$

In Subsection IV-B, we will present the proposed sparse channel scheme to address these insignificant elements and determine k_ν .

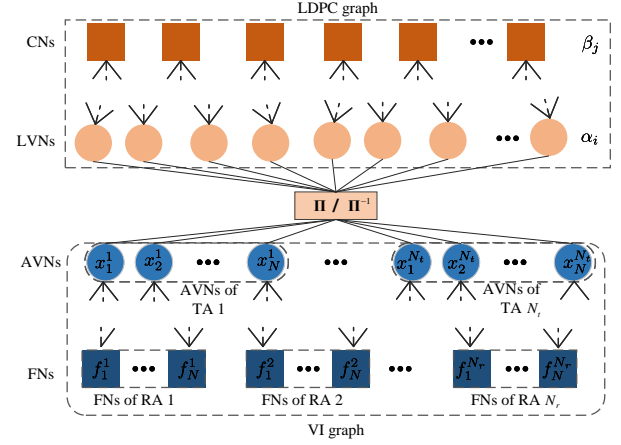


Fig. 4: Factor graph representation of the proposed JSG.

A factor graph is a bipartite graph representing the factorization of a joint distribution function $p(\mathbf{x}, \mathbf{y})$. Fig. 3(a) shows an example of $\bar{\mathbf{H}}_p$ in a SISO-AFDM system with $N = 16$ and $k_\nu = 2$. Consider the one-path channel in Fig. 3(a), the factor graph is shown in Fig. 3(b). Each AFDM variable node (AVN) is connected to $2k_\nu + 1$ function nodes (FNs) and each FN is also occupied by $2k_\nu + 1$ AVNs. For simplicity, denote x_m^t as the transmitted symbol at the m th SC of the t th TA. Consider the MIMO-AFDM of Scenario 1, the joint distribution $p(\mathbf{x}, \mathbf{y})$ can be factorized as

$$\begin{aligned} p(\mathbf{y}, \mathbf{x}) &= p(\mathbf{y}|\mathbf{x})p(\mathbf{x}) \\ &= \prod_{t=1}^{N_t} \prod_{m=1}^N p(x_m^t) \prod_{r=1}^{N_r} \prod_{n=1}^N p(y_n^r|\mathbf{x}), \end{aligned} \quad (18)$$

where $p(y_n^r|\mathbf{x}) = \mathcal{CN}(y_n^r; \sum_t \sum_m h_{n,m}^{r,t} x_m^t, N_0)$, $h_{n,m}^{r,t}$ denotes the channel coefficient from the m th SC of the t th TA to the n th SC of the r th RA, and $p(x_m^t)$ denotes the prior probability of x_m^t . The factor graph can be designed to contain NN_t AVNs x_m^t and $N_r N$ likelihood FNs f_m^r . The LDPC codes can also be represented by a bipartite graph called Tanner graph with the belief messages passing over the LDPC VNs (LVNs) and LDPC check nodes (CNs). In this paper, we propose to design the JSG-based receiver by merging the VI factor graph and the LDPC graph into an integrated one. As a result, the belief messages are exchanged iteratively on a JSG. Fig. 4 shows an example of the JSG for the MIMO-AFDM of Scenario 1. The AVNs and FNs represent the transmit layers and the likelihood function $p(y_n^r|\mathbf{x})$. The set of AVN indices sharing the n th FN of the r th RA is denoted as $F(n, r) = \{(m, t) : h_{n,m}^{r,t} \neq 0\}$, whereas the set of FN indices sharing the m th VN is denoted by $V(m, t) = \{n, r : h_{n,m}^{r,t} \neq 0\}$. In addition, the cardinalities of $V(m, t)$ and $F(n, r)$ are denoted as $|V(m, t)| = d_f$ and $|F(n, r)| = d_v$, respectively. In this paper, we first consider the MIMO-AFDM in Scenario 1, and the results can be readily extended to Scenario 2.

C. BP-JSG

In this subsection, we first consider the optimization metric as the exclusive KL divergence, i.e., $\text{KL}(p|q)$. It is well known

that the $\log(\cdot)$ partition function $\log p(\mathbf{y})$ can be decomposed as [37]

$$\begin{aligned} \log p(\mathbf{y}) &= \sum_{\mathbf{x}} q(\mathbf{x}) \log \left(\frac{p(\mathbf{x}, \mathbf{y})}{q(\mathbf{x})} \times \frac{q(\mathbf{x})}{p(\mathbf{x}|\mathbf{y})} \right) \\ &= \underbrace{\sum_{\mathbf{x}} q(\mathbf{x}) \log p(\mathbf{x}, \mathbf{y}) - \sum_{\mathbf{x}} q(\mathbf{x}) \log q(\mathbf{x}) + \text{KL}(q|p)}_{\mathcal{L}_{\text{ELBO}}}, \quad (19) \end{aligned}$$

where $\mathcal{L}_{\text{ELBO}}$ is the evidence lower bound (ELBO). Namely, $\mathcal{L}_{\text{ELBO}} = \log p(\mathbf{y}) - \text{KL}(q|p)$. As a result, instead of minimizing $\text{KL}(p|q)$, one can maximize $\mathcal{L}_{\text{ELBO}}$. To solve this problem, we resort to the Bethe approximation for maximizing $\mathcal{L}_{\text{ELBO}}$. It is shown that the stationary points of the Bethe approximation to the $\mathcal{L}_{\text{ELBO}}$ are equivalent to the fixed points of the standard BP algorithm [34], [37], [38]. Denote $L_{v_m^t \rightarrow f_n^r}^l(x_m^t)$ and $L_{f_n^r \rightarrow v_m^t}^l(x_m^t)$ as the LLR propagated from VN v_m^t to FN f_n^r and FN f_n^r to VN v_m^t at the l th iteration, respectively. The iterative messages exchanged between FNs and AVNs are computed as

$$\begin{aligned} L_{f_n^r \rightarrow v_m^t}^l(x_m^t) &= \max_{\forall x_{m'}^t, x_{m''}^t \neq x_m^t} -\frac{1}{2N_0} \left| y_k - \sum_{m,t \in F(n,r)} h_{n,m}^{r,t} x_m^t \right|^2 \\ &\quad + \sum_{m,t \in F(n,r)} L_{v_m^t \rightarrow f_n^r}^l(x_m^t), \quad (20) \end{aligned}$$

where

$$L_{v_m^t \rightarrow f_n^r}^l(x_m^t) = \sum_{n,r \in V(m,t) \setminus \{n,r\}} I_{f_n^r \rightarrow v_m^t}^{l-1}(x_m^t), \quad (21)$$

where $n, r \in V(m,t) \setminus \{n,r\}$ represents removing the FN f_n^r from the set $V(m,t)$.

The message propagation within the LDPC graph and between the LDPC and VI graph will be discussed along with the proposed EP-JSG.

D. EP-JSG

In BP-JSG, (20)-(21) require global searches over the joint space of all symbols, which is a discrete set. Consequently, the computational complexity of BP-JSG is exponential, i.e., $\mathcal{O}(M^{P k_\nu})$. As M , P , and k_ν increase, BP-JSG becomes impractical in real-world systems, especially in scenarios with high mobility and rich scattering environments as P and k_ν typically have large values. Instead of using $\text{KL}(q|p)$, we resort to the inclusive $\text{KL}(p|q)$ as the optimization metric. The objective is to find a distribution family $q(\mathbf{x})$ that minimizes $\text{KL}(p|q)$. Although global optimization is intractable, it can be iteratively solved using the well-known EP algorithm [34], [38], [39]. Denote $I_{v_m^t \rightarrow f_n^r}^l(x_m^t)$ and $I_{f_n^r \rightarrow v_m^t}^l(x_m^t)$ as the belief messages propagated from VN v_m^t to FN f_n^r and f_n^r to v_m^t at the l th iteration, respectively. According to the EP principles, the message update rule can be expressed as [39]

$$I_{v_m^t \rightarrow f_n^r}^l(x_m^t) \propto \frac{\text{Proj}_\Phi(q_0^l(x_m^t))}{I_{f_n^r \rightarrow v_m^t}^{l-1}(x_m^t)}, \quad (22)$$

$$I_{f_n^r \rightarrow v_m^t}^l(x_m^t) \propto \frac{\text{Proj}_\Phi(q_{n,r}^t(x_m^t))}{I_{v_m^t \rightarrow f_n^r}^l(x_m^t)}, \quad (23)$$

where $\text{Proj}_\Phi(p) = \arg \min_{q \in \Phi} \text{KL}(p|q)$ denotes the projection of a particular distribution p into some distribution set Φ for the given metric of $\text{KL}(p|q)$, and

$$q_0^l(x_m^t) \propto p_0(x_m^t) \prod_{r=1}^{N_r} \prod_{n,r \in V(m,t)} I_{f_n^r \rightarrow v_m^t}^l(x_m^t), \quad (24)$$

$$q_{n,r}^t(x_m^t) \propto \sum_{x_{m'}^t \neq x_m^t} p(y_n^r | x_{m'}^t) \prod_{m,t \in F(n,r) \setminus \{m,t\}} I_{v_m^t \rightarrow f_n^r}^l(x_m^t). \quad (25)$$

The above procedure can be understood as the messages propagation over the VI graph depicted in Fig. 4. It treats the messages exchanged between VNs and FNs as continuous random variables and approximates the true distribution with a Gaussian distribution, characterized by its mean and variance. This approach enables signal detection to be transformed into the computation of mean and variance, avoiding the need to traverse all symbols. Specifically, we have

$$\text{Proj}_\Phi(q_0^l(x_m^t)) \propto \mathcal{CN}(\mu_{m,t}^l, \xi_{m,t}^l), \quad (26a)$$

$$I_{v_m^t \rightarrow f_n^r}^l(x_m^t) \propto \mathcal{CN}(\mu_{m,t \rightarrow n,r}^l, \xi_{m,t \rightarrow n,r}^l), \quad (26b)$$

$$I_{f_n^r \rightarrow v_m^t}^l(x_m^t) \propto \mathcal{CN}(\mu_{n,r \rightarrow m,t}^l, \xi_{n,r \rightarrow m,t}^l). \quad (26c)$$

Now, we introduce the detailed message propagation in the proposed JSG.

1) *Updating of VNs*: In the separate graph case, VNs only gather information from one type of nodes (FNs or CNs). However, in the JSG, the updating of VNs in JSG involves the information from both sub-graphs. Let $L_{\alpha_i \rightarrow \beta_j}$ be $L_{\beta_j \rightarrow \alpha_i}$ by the LLR updating from the LVN α_i to the CN β_j , and the β_j to the α_i , respectively. Then, the updated $L_{\alpha_i \rightarrow \beta_j}$ is given by

$$L_{\alpha_i \rightarrow \beta_j} = L_{\alpha_i}^{a, \text{LDPC}} + \sum_{j' \in \eta_i \setminus j} L_{\beta_{j'} \rightarrow \alpha_i}, \quad (27)$$

where $L_{\alpha_i}^{a, \text{LDPC}}$ denotes the *a priori* LLR updated from VI graph at the LVN α_i , and η_i denotes the set of CNs connected to LVN α_i .

Denote $L^{a, \text{VI}}(x_m^t)$ as the *a priori* LLR updated from LDPC graph to AVN x_m^t . The AVN nodes gather the LLR information from both the LDPC graph and FNs as follows

$$Lq(x_m^t | \mathbf{y}) = L^{a, \text{VI}}(x_m^t) + \sum_{(n,r) \in V(m,t)} L_{f_n^r \rightarrow v_m^t}^l(x_m^t). \quad (28)$$

Then, based on (28), the *a posteriori* belief probability for AVN x_m^t can be calculated as

$$p(x_m^t | \mathbf{y}) = \frac{\exp(Lq(x_m^t | \mathbf{y}))}{1 + \exp(Lq(x_m^t | \mathbf{y}))}. \quad (29)$$

Accordingly, the mean and variance of AVN x_m^t can be expressed as

$$\begin{aligned} \mu_{m,t}^l &= \sum_{a_m^t \in \mathcal{X}} p(x_m^t = a_m^t | \mathbf{y}) a_m^t, \\ \xi_{m,t}^l &= \sum_{a_m^t \in \mathcal{X}} p(x_m^t = a_m^t | \mathbf{y}) \left| a_m^t - \mu_{m,t}^l \right|^2. \quad (30) \end{aligned}$$

Upon obtaining the mean $\mu_{m,t}^l$ and variance $\xi_{m,t}^l$, by substituting (26a)-(26c) into (22), one has the mean and variance passing from VNs to FNs respectively as follows

$$\begin{aligned}\xi_{m,t \rightarrow n,r}^l &= \left(\frac{1}{\xi_{m,t}^l} - \frac{1}{\xi_{n,r \rightarrow m,t}^{l-1}} \right)^{-1}, \\ \mu_{m,t \rightarrow n,r}^l &= \xi_{m,t \rightarrow n,r}^l \left(\frac{\mu_{m,t}^l}{\xi_{m,t}^l} - \frac{\mu_{n,r \rightarrow m,t}^{l-1}}{\xi_{n,r \rightarrow m,t}^{l-1}} \right).\end{aligned}\quad (31)$$

2) *Updating of FNs and CNs*: The LLR of the CN β_j is updated as

$$L_{\beta_j \rightarrow \alpha_i} = \gamma^{-1} \left(\sum_{i' \in \phi_j \setminus i} \gamma(L_{\alpha_{i'} \rightarrow \beta_j}) \right), \quad (32)$$

where $\phi_j \setminus i$ is the set of VNs (excluding α_i) that connect to the CN β_j , and $\gamma(x)$ and $\gamma^{-1}(x)$ are respectively defined as

$$\begin{aligned}\gamma(x) &= \text{sign}(x) \times \left(-\log \tan \frac{|x|}{2} \right), \\ \gamma^{-1}(x) &= (-1)^{\text{sign}(x)} \times \left(-\log \tan \frac{|x|}{2} \right),\end{aligned}\quad (33)$$

where $\text{sign}(x)$ denotes the the sign of x .

On the FN side, the calculation of $\mu_{n,r \rightarrow m,t}^l$ and $\xi_{n,r \rightarrow m,t}^l$ plays a crucial role in the convergence of expectation propagation. The received signal y_n^r is considered as the sum of transmitted signals from all layers plus the noise. Namely, we have

$$x_m^t = \frac{1}{h_{n,m}^{r,t}} \left(y_n^r - \sum_{\substack{i,j \in F(n,r), \\ i \neq m, j \neq t}} h_{n,i}^{r,j} x_i^j + \omega_n^r \right). \quad (34)$$

Then, based on (26a)-(26c) and (25), the message in the reverse direction becomes

$$\mu_{n,r \rightarrow m,t}^l = \frac{y_n^r - Z_{n,r \rightarrow m,t}^l}{h_{n,m}^{r,t}}, \quad \xi_{n,r \rightarrow m,t}^l = \frac{N_0 + B_{n,r \rightarrow m,t}^l}{|h_{n,m}^{r,t}|^2}, \quad (35)$$

where

$$\begin{aligned}Z_{n,r \rightarrow m,t}^l &= \sum_{\substack{i,j \in F(n,r), \\ i \neq m, j \neq t}} h_{n,i}^{r,j} \mu_{i,j \rightarrow n,r}^{l-1}, \\ B_{n,r \rightarrow m,t}^l &= \sum_{\substack{i,j \in F(n,r), \\ i \neq m, j \neq t}} |h_{n,i}^{r,j}|^2 \xi_{i,j \rightarrow n,r}^{l-1}.\end{aligned}\quad (36)$$

Finally, the posterior probabilities of transmitted symbol in LLR domain is given by

$$L_{f_n^r \rightarrow v_m^t}^l(a_m^t) = \frac{-|a_m^t - \mu_{n,r \rightarrow m,t}^l|^2}{\xi_{n,r \rightarrow m,t}^l}, \quad \forall a_m^t \in \mathcal{X}. \quad (37)$$

3) *Extrinsic and prior LLRs exchange*: The output extrinsic information of the VI detector are utilized as the *a priori* LLRs for the LDPC decoder. Specifically, the extrinsic information at the AVN x_m^t is calculated as

$$L_{m,t}^{e,VI}(a_m^t) = \sum_{r=1}^{N_r} \sum_{n=1}^N L_{f_n^r \rightarrow v_m^t}^l(a_m^t). \quad (38)$$

Denote $\mathbf{c}_{m,t} = \{c_{m,t}^i | i = 1, 2, \dots, \log_2 M\} \in \mathbb{B}^{\log_2 M \times 1}$ as the corresponding bits of the symbol a_m^t . Then, $L_{m,t}^{e,VI}(a_m^t)$

is further demapped to the bit-level LLRs, which can be expressed as

$$L_{m,t}^{e,VI}(c_{m,t}^i) = \log \frac{\sum_{\forall \mathbf{c}_{m,t}: c_{m,t}^i=0} \exp(L_{m,t}^{e,VI}(a_m^t))}{\sum_{\forall \mathbf{c}_{m,t}: c_{m,t}^i=1} \exp(L_{m,t}^{e,VI}(a_m^t))}. \quad (39)$$

Let $L_{m,t}^{e,VI}(\mathbf{c})$ denote the extrinsic bit LLRs from N_t transmit antennas. $L_{m,t}^{e,VI}(\mathbf{c})$ is further deinterleaved as the *a priori* LLRs input to the LDPC decoder, i.e.,

$$L^{a,LDPC}(\boldsymbol{\alpha}) = \Pi^{-1} \left(L_{m,t}^{e,VI}(\mathbf{c}) \right). \quad (40)$$

At the LVN side, it gathers information from CNs by

$$L^{e,LDPC}(\alpha_i) = \sum_{j \in \eta_i} L_{\beta_j \rightarrow \alpha_i}. \quad (41)$$

After interleaving, the resultant LLR can be expressed as

$$L^{a,VI}(\mathbf{c}) = \Pi(L^{e,LDPC}(\boldsymbol{\alpha})). \quad (42)$$

To pass the belief messages from LVNs to AVNs, one needs to transform bit LLRs to symbol LLRs. Specifically, the *a priori* symbol-level LLRs can be calculated as

$$L^{a,VI}(x_m^t) = \sum_{i=1}^{\log_2(M)} \log \frac{\exp(-\Psi_{\mathcal{X}}[i] L_{\alpha}^{a,VI}(c_{m,t}^i))}{1 + \exp(L_{\alpha}^{a,VI}(c_{m,t}^i))}, \quad (43)$$

where $\Psi_{\mathcal{X}}[i] \in \{0, 1\}$ denotes the labeling value of the i th bit of \mathcal{X} .

Remark 1: The proposed JSG allows belief messages from the LDPC and VI graphs to propagate in a joint manner. In addition, the AVNs (FNs) and LVNs (CNs) are able to update messages simultaneously, leading to faster convergence with fewer iterations.

IV. THE PROPOSED E-JSG

Note that messages in the VI graph are updated at the symbol level, whereas messages in the LDPC graph are updated on a per-bit basis. This mismatch between symbol-level message updates in the VI graph and bit-level updates in the LDPC graph results in inefficient message propagation. Furthermore, the computation of bit-to-symbol and symbol-to-bit LLRs introduces higher computational complexity.

To address these challenges, we propose an E-JSG, which enables message updating on a per-bit basis. Moreover, to further reduce computational complexity, we introduce a sparse channel method based on the eSNR, which helps eliminate unnecessary message propagation over the E-JSG.

A. The Proposed E-JSG

1) *Linear encoding-inspired VI graph design*: Let us consider the linear encoding for a modulation process in the following way [40]

$$\mathbf{x} = \mathbf{g}\mathbf{u}, \quad (44)$$

where $\mathbf{g} = [g_1, g_2, \dots, g_{\log_2 M}]$ denotes the constellation generator vector and $\mathbf{u} = [u_1, u_2, \dots, u_{\log_2 M}]^T \in \{1, -1\}^{\log_2 M}$ stands for the instantaneous input binary message vector. By including all the \mathbf{u} 's according to its corresponding integer values in ascending order, we obtain a $\log_2 M \times M$ matrix \mathbf{U} . For example, when $M = 4$, we have

$$\mathbf{U} = \begin{bmatrix} - & + & - & + \\ + & - & + & - \end{bmatrix}, \quad (45)$$

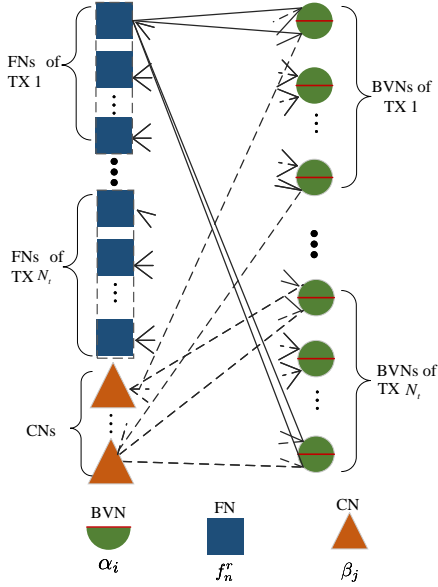


Fig. 5: Factor representation of the proposed E-JSG.

where “+” and “-” denote +1 and -1, respectively. Hence, the signal model of (10) can be rewritten as

$$\mathbf{y}_r = \sum_{t=1}^{N_t} \mathbf{H}^{(r,t)} \mathbf{G} \mathbf{u}_t + \mathbf{w}_r = \sum_{t=1}^{N_t} \bar{\mathbf{H}}^{(r,t)} \mathbf{u}_t + \mathbf{w}_r, \quad (46)$$

where $\mathbf{u}_t \in \{1, -1\}^{N \log_2 M \times 1}$ denotes the instantaneous input binary message vector of an AFDM symbol at the t th TA, $\mathbf{G} = [\mathbf{g}^T, \dots, \mathbf{g}^T]^T \in \mathbb{C}^{N \times N \log_2 M}$ denotes the linear

encoding matrix, and $\bar{\mathbf{H}}^{(r,t)} = \mathbf{H}^{(r,t)} \mathbf{G}$ denotes the combined channel matrix. By utilizing (46), the VI graph designed only contains bit VNs (BVNs) instead of the symbol VN. Hereafter, the VNs in the E-JSG are referred to as the BVNs. As a result, the LLR calculation for bit to symbol is no longer required and the interleaver (deinterleaver) can also be eliminated. Fig. 5 shows an example of a folded view of the proposed E-JSG, where $M = 4$ is considered. Based on the JSG framework introduced in Section III, both FNs and CNs are able to update their messages concurrently. Subsequently, the BVNs of VI and LDPC subgraphs simultaneously update the mean and variance, and LLR to FNs and CNs, respectively. Therefore, it is reasonable to place FNs (rectangles) and CNs (triangles) on one side, while drawing BVNs (circles) on the other side. Note that one circle contains $\log_2 M$ BVNs.

In the following, we present the message propagation in the proposed E-JSG.

2) *Update of BVNs to CNs and FNs:* The updating of i th BVN α_i to the j th CN β_j can be calculated as

$$L_{\alpha_i \rightarrow \beta_j} = \sum_{(r,n) \in V(i)} L_{f_n^r \rightarrow \alpha_i} + \sum_{j' \in \eta_i \setminus j} L_{\beta_{j'} \rightarrow \alpha_i}, \quad (47)$$

where $V(i)$ is the set of FNs connected to the i th BVN. Similarly, to update the BVNs to FNs, the BVNs gather the information from both sides, i.e.,

$$L_{\alpha_i} = \sum_{(r,n) \in V(i)} L_{f_n^r \rightarrow \alpha_i} + \sum_{i \in \phi_j} L_{\alpha_i \rightarrow \beta_j}. \quad (48)$$

Algorithm 1 Message Propagation in the Proposed E-JSG

- 1: **Initialize** : $L_{\beta_j \rightarrow \alpha_i} = 0$, $L_{f_n^r \rightarrow \alpha_i} = 0$, $L_{\alpha_i \rightarrow \beta_j} = 0$, $L_{\alpha_i \rightarrow f_n^r} = 0$, $\mu_{n,r \rightarrow i}^0 = 0$, $\xi_{n,r \rightarrow i}^0 = 10$, $\mu_{i \rightarrow n,r}^0 = 0$, $\xi_{i \rightarrow n,r}^0 = 10$, and $\forall i, \forall j, \forall n, \forall r$.
- 2: **for** $l = 1 : L_t$ **do**
- 3: **Step 1 : BVNs update**
- 4: Update $L_{\alpha_i \rightarrow \beta_j}$ based on (47)
- 5: Update L_{α_i} based on (48)
- 6: Update the mean and variance at the BVN, i.e., $\xi_{i \rightarrow n,r}^l$ and $\mu_{i \rightarrow n,r}^l$, according to (50)
- 7: **Step 2 : FNs and CNs update**
- 8: Update $L_{\beta_j \rightarrow \alpha_i}$ according to (32)
- 9: Update $\mu_{n,r \rightarrow i}^l$ and $\xi_{n,r \rightarrow i}^l$ according to (51)
- 10: Update $L_{f_n^r \rightarrow \alpha_i}$ according to (53)
- 11: **end for**
- 12: **Output** : L_{α_i}

In this paper, we consider $M = 4$ with $\mathbf{g} = [1, -1j]$. Then, the calculation of mean and variance of the i th BVN can be simplified as

$$\begin{aligned} \mu_i^l &= 1 - 2p(\alpha_i^l = -1 | \mathbf{y}) = \frac{1 - \exp(L_{\alpha_i})}{1 + \exp(L_{\alpha_i})}, \\ \xi_i^l &= \sum_{a_i \in \{-1, 1\}} p(\alpha_i^l = a_i | \mathbf{y}) |a_i - \alpha_i^l|^2 = \alpha_i^l (\alpha_i^l - 1)^2. \end{aligned} \quad (49)$$

One has the the mean and variance passing from VNs to FNs respectively as follows

$$\begin{aligned} \xi_{i \rightarrow n,r}^l &= \left(\frac{1}{\xi_i^l} - \frac{1}{\xi_{n,r \rightarrow i}^{l-1}} \right)^{-1}, \\ \mu_{i \rightarrow n,r}^l &= \xi_{i \rightarrow n,r}^l \left(\frac{\mu_i^l}{\xi_i^l} - \frac{\mu_{n,r \rightarrow i}^{l-1}}{\xi_{n,r \rightarrow i}^{l-1}} \right). \end{aligned} \quad (50)$$

3) *Update of CNs and FNs to BVNs:* The update for CNs are the same as that in (32) and (33). For the mean and variance update in the opposite direction, similar to (26a)-(26c) and (25), we have

$$\mu_{n,r \rightarrow i}^l = \frac{y_n^r - \bar{Z}_{n,r \rightarrow i}^l}{\bar{h}_{n,r}^i}, \quad \xi_{n,r \rightarrow i}^l = \frac{N_0 + \bar{B}_{n,r \rightarrow i}^l}{|\bar{h}_{n,r}^i|^2}, \quad (51)$$

where $\bar{h}_{n,r}^i$ is the effective channel coefficient from the i th BVN to the FN f_n^r as specified in (46), and

$$\begin{aligned} \bar{Z}_{n,r \rightarrow i}^l &= \sum_{\substack{i \in \bar{F}(n,r) \\ i \neq i}} \bar{h}_{n,r}^{i'} \mu_{i \rightarrow n,r}^{l-1}, \\ \bar{B}_{n,r \rightarrow i}^l &= \sum_{\substack{i \in \bar{F}(n,r) \\ i \neq i}} |\bar{h}_{n,r}^{i'}|^2 \xi_{i \rightarrow n,r}^{l-1}. \end{aligned} \quad (52)$$

Finally, the posterior probabilities of the transmitted symbol in LLR domain is given by

$$L_{f_n^r \rightarrow \alpha_i} = \frac{-|1 + \mu_{n,r \rightarrow i}^l|^2 + |1 - \mu_{n,r \rightarrow i}^l|^2}{\xi_{n,r \rightarrow i}^l} = -\frac{4\mu_{n,r \rightarrow i}^l}{\xi_{n,r \rightarrow i}^l}. \quad (53)$$

The overall message propagation of the proposed E-JSG is summarized in Algorithm (1).

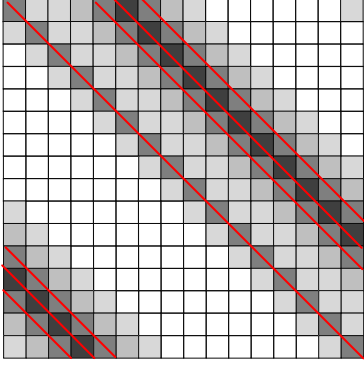


Fig. 6: An example of the selected entries, highlighted by the red lines, for message propagation of a two-path channel.

B. Sparse Channel Based on eSNR

In the proposed JSG and E-JSG, the computational complexity depends crucially on the degree at each FN, which is determined by P and κ_ν . Specifically, the degree at each FN of E-JSG is upper bounded by $P\kappa_\nu \log_2(M)$. In general, P and κ_ν tend to be relatively large, particularly in rich scattering scenarios and when fractional Doppler shift is significant. To reduce the computational complexity of the JSG and E-JSG, one possible approach is to reduce the number of edges of the VI graph, i.e., select a small value of κ_ν for each $\bar{\mathbf{H}}_p$, thereby reducing unnecessary message propagation. This is reasonable as some of the non-zero elements in \mathbf{H} has very small amplitude, the message propagating over the corresponding edges may not significantly improve the error rate performance. To this end, we propose a sparse channel method based on eSNR to determine the nonzero elements for message passing, which is equivalent to determine k_ν , and to approximate multiple graph edges with insignificant channel coefficients as a single edge on the VI graph.

Denote the set of non-zero channel coefficients at the FN f_n^r as $\mathcal{D}(n, r)$, and let $D = |\mathcal{D}(n, r)|$ return the cardinalities of $\mathcal{D}(n, r)$. Then, we sort the D non-zero channel coefficients in descending order and choose the D_L largest terms, denoted as $D_L(n, r)$, for message propagation over the VI graph. We further denote $D_S(n, r)$ as the remaining terms. Then, the edges corresponding to the $D_S(n, r)$ are approximated as a single edge. Consequently, the means and variance in (51) and (52) are computed respectively as follows

$$\begin{aligned} \bar{Z}_{n,r \rightarrow i}^l &= \sum_{\substack{i \in D_L(n,r), \\ i \neq i}} \bar{h}_{n,r}^i \mu_{i \rightarrow n,r}^{l-1} + \mu_{S \rightarrow n,r}^{l-1} \sum_{i \in D_S(n,r)} \bar{h}_{n,r}^i, \\ \bar{B}_{n,r \rightarrow i}^l &= \sum_{\substack{i \in D_L(n,r), \\ i \neq i}} |\bar{h}_{n,r}^i|^2 \xi_{i \rightarrow n,r}^{l-1} + \xi_{S \rightarrow n,r}^{l-1} \sum_{i \in D_S(n,r)} |\bar{h}_{n,r}^i|^2. \end{aligned} \quad (54)$$

By approximating the insignificant edges as a single edge, it allows more efficient message passing. In what follows, we present the selection of $D_L(n, r)$ based on eSNR. We first define the elements at the n th row and $m = (n + s)_N$ th column of $\mathbf{H}^{(r,t)}$ as the elements in its s th cyclic-shift, where $0 \leq s \leq N - 1$. To maintain a regular structure of E-JSG, as per equation (10), all elements at the s th cyclic-shift are either added to $D_L(n, r)$ or $D_S(n, r)$ for approximation. It

should be noted that for each $\bar{\mathbf{H}}_p$, we have $|\bar{\mathbf{H}}_p[n, m]| = |\bar{\mathbf{H}}_p[n', m']|$, where $m = (n + s)_N$, $m' = (n' + s)_N$, and $0 \leq s \leq N - 1$. However, this may not hold for $\mathbf{H}^{(r,t)}$ as the phase of $\bar{\mathbf{H}}_p$ changes along with the positions of $m = (n + s)_N$, leading to $|\mathbf{H}^{(r,t)}[n, m]| \neq |\mathbf{H}^{(r,t)}[n', m']|$ when the fractional Doppler and multipath exist. Hence, we define the average channel gain at the s th cyclic-shift as $G_s = \frac{1}{N} \sum_{n=1}^N |\mathbf{H}^{(r,t)}[n, (n' + s)_N]|^2$. The elements at the s th cyclic-shift is added into $D_L(n, r)$ for message propagation if and only if the eSNR of the s th cyclic-shift is larger than a threshold, i.e.,

$$\text{eSNR}_s \equiv 10 \log \frac{G_s}{N_0} \geq \text{eSNR}_{\text{th}}, 0 \leq s \leq N - 1, \quad (55)$$

where eSNR_{th} denotes the threshold, and eSNR_s denotes the eSNR at the s th cyclic-shift. Fig. 6 shows an example of the selected entries for message propagation of a two-path channel with $N = 16$. The elements at the $s = 0, 4, 5$ and 6 cyclic-shifts are added to $D_L(n, r)$ for message propagation.

C. Complexity Analysis

In this subsection, we first analyze the computational complexity of the proposed E-JSG. We then discuss the decoding latency.

1) *Computational complexity*: The computation of (20) requires $\sum_{n=1}^{N_F} 2d_f^n M^{d_f^n}$ complex-valued multiplications and $\sum_{n=1}^{N_F} M^{d_f^n}$ complex-valued additions at each iteration, where d_f^n denotes the number edges connected to the n th FN and N_F denotes the number of FNs. In addition, the calculation of (21) requires $N_V(Md_v^{\text{ave}} - 1)$ complex-valued additions, where $d_v^{\text{ave}} = \frac{1}{N_V} \sum_{m=1}^{N_V} d_v^m$ denotes the average degrees of the VNs and N_V denotes the number of VNs. Note that the output symbol LLRs are further demapped to bit-level LLRs based on (39), which requires $2N_V \log_2 M$ real-valued additions, $N_V M$ exponentials, and $N_V \log_2 M \log(\cdot)$ calculations. The bit-level LLRs to symbol level LLRs of (43) requires about $2 \log_2 M$ exponentials, $\log_2 M \log(\cdot)$ calculations and $2 \log_2 M$ additions.

The messaging passing of VI graph with EPA principle has linear computational complexity with most of the key parameters, i.e., M , N_t , N_r and N . The update of mean and variance at from AVN to FN requires about $Md_v^m + 2M + 3$ additions, $2M$ exponentials, $3M + 8$ multiplications at the m th AVN. Moreover, the update of mean and variance from the n th FN to AVN requires about $2d_f^n + 2 + M$ additions, $3d_f + 3 + 2M$ multiplications. Similarly, one can obtain the computational complexity for the proposed E-JSG. The computational complexity of different receivers are summarized in Table I, where $d_f^{\text{ave}} = \frac{1}{N_F} \sum_{n=1}^{N_F} d_f^n$. Since the complexities of the LDPC decoding are the same for different receivers, they are thus omitted in Table I.

2) *Detection and decoding latency*: In practical systems, the detection and decoding latency are mainly dominated by the iterative structures of the receiver. We assume that the receiver is equipped with powerful processing units, and parallel computation techniques are also applied to reduce the detection and decoding latency. The conventional MMSE with LDPC decoder, denoted as MMSE-LDPC, and the turbo

TABLE I: Computational complexity

Algorithm	Real-valued multiplications	Real-valued addition	Exponentials	Log(\cdot)	De-interleaving, interleaving ?
MMSE	$6N^3 + 2N^2 + 2N$	-	$2N_V(\log_2 M + M)$	$2N_V \log_2 M$	Yes
BP-JSG	$4 \sum_{n=1}^{N_F} d_f^{2n} M^{d_f^{2n}}$	$2 \left(\sum_{n=1}^{N_F} M^{d_f^{2n}} + N_V(Md_v^{\text{ave}} + 3 \log_2 M - 1) \right)$	$2N_V(\log_2 M + M)$	$2N_V \log_2 M$	Yes
EP-JSG	$4(N_V(3M + 8) + N_F(3d_f^{\text{ave}} + 3 + 2M))$	$2(N_V(Md_v^{\text{ave}} + 2M + 3) + N_F(2d_f^{\text{ave}} + 2 + M))$	$2N_V(\log_2 M + 3M)$	$2N_V \log_2 M$	Yes
E-JSG	$N_V \log_2 M(d_v^{\text{ave}} + 7)$	$8N_V \log_2 M + 6N_F \log_2 M d_f^{\text{ave}}$	$N_V \log_2 M$	-	No

receiver with iterative detection and decoding (Turbo-IDD) are employed as the benchmarks for comparisons. In the Turbo-IDD structure, iterative messages are exchanged between the detector and channel decoder [29]. Denote T_{VI}^{VN} and T_{VI}^{FN} as the average run time for the messaging propagation at the VNs and FNs of the VI graphs, respectively. Similar, let T_{LDPC}^{VN} and T_{LDPC}^{CN} be the average run time for the messaging propagation at the VNs and CNs of the LDPC graph, respectively. Therefore, the detection and decoding latency for the MMSE-LDPC receiver can be approximated as

$$T_{\text{MMSE-LDPC}} = T_{\text{MMSE}} + N_{\text{LDPC}}(T_{\text{LDPC}}^{\text{VN}} + T_{\text{LDPC}}^{\text{CN}}) + T_{\text{MMSE}}^{\text{res}}, \quad (56)$$

where N_{LDPC} denotes the number of iterations of the LDPC decoding, and $T_{\text{SSD}}^{\text{res}}$ denotes the residential run time, such as the symbol to LLR transformation and interleaving. Similarly, the detection and decoding latency for the Turbo-IDD receiver can be expressed as

$$T_{\text{IDD}} = N_{\text{out}}(N_{\text{VI}}(T_{\text{VI}}^{\text{VN}} + T_{\text{VI}}^{\text{FN}}) + N_{\text{LDPC}}(T_{\text{LDPC}}^{\text{VN}} + T_{\text{LDPC}}^{\text{CN}}) + T_{\text{IDD}}^{\text{res}}), \quad (57)$$

where N_{out} denotes the outer iteration of the Turbo-IDD receiver, N_{VI} and N_{LDPC} denote the number of iterations of the VI detection and LDPC decoding, respectively, and $T_{\text{IDD}}^{\text{res}}$ denotes the residential run time. In addition, the detection and decoding latency for the proposed VI-JSG and E-JSP can be respectively expressed as

$$T_{\text{JSG}} = N_{\text{JSG}} \left(\max \{ T_{\text{VI}}^{\text{VN}}, T_{\text{LDPC}}^{\text{VN}} \} + \max \{ T_{\text{VI}}^{\text{FN}}, T_{\text{LDPC}}^{\text{CN}} \} + T_{\text{JSG}}^{\text{res}} \right), \quad (58)$$

and

$$T_{\text{E-JSG}} = N_{\text{E-JSG}} \left(\max \{ T_{\text{VI}}^{\text{VN}}, T_{\text{LDPC}}^{\text{VN}} \} + \max \{ T_{\text{VI}}^{\text{FN}}, T_{\text{LDPC}}^{\text{CN}} \} \right). \quad (59)$$

where N_{JSG} and $N_{\text{E-JSG}}$ denote the number of iterations for the proposed JSG and E-JSG receivers, respectively.

V. NUMERICAL RESULTS

This section presents numerical simulation results to validate the performance of the proposed receivers in MIMO-AFDM systems. For system setting, we set $N = 128$, $c_1 = c_2 = \frac{1}{N}$, and $N_{\text{CPP}} = 24$. Two maximum normalized Doppler values are considered, i.e., $\nu_{\text{max},p} = 0.075$ and 1.2. In addition, we set $N_{\text{VI}} = 3$, $N_{\text{LDPC}} = 3$ and $N_{\text{out}} = 4$ for Turbo-IDD receivers. The number of iterations for both the proposed JSG and the channel decoder in the MMSE-LDPC is set to 12. The 5G NR LDPC code with a length of 512 and rate of 0.5 is considered. Specifically, base graph 2 is used, with LVN and CN degree distributions given by $\lambda(x) = 0.4x^2 + 0.4x^3 + 0.2x^5$

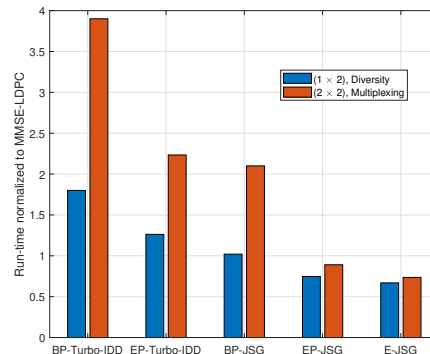


Fig. 7: Normalized run-time complexity to MMSE-LDPC.

and $\rho(x) = 0.5x^6 + 0.5x^7$, respectively, as specified in 3GPP TS-38.212 [41].

We first evaluate the run-time complexity as the approximation of the detection and decoding latency of various receivers. Specifically, the run-time parameters of $T_{\text{MMSE}}^{\text{res}}$ in (56)-(59) are estimated in the Matlab platform with an i7 processor. Fig. 7 shows the normalized run-time complexity of MMSE-LDPC of different receivers, i.e., $T_{\text{IDD}}/T_{\text{MMSE-LDPC}}$, $T_{\text{JSG}}/T_{\text{MMSE-LDPC}}$ and $T_{\text{E-JSG}}/T_{\text{MMSE-LDPC}}$. As can be seen from the figure, the BP-Turbo-IDD receiver exhibits the highest run-time complexity, whereas the proposed E-JSG receiver benefits from the lowest run-time complexity.

We now evaluate the performance of MIMO-AFDM with different receivers over multi-path fading channels. Specifically, we consider a two-path and a four-path channel without Doppler effects, where the delay taps are assumed to be randomly located within $[0, 6]$ and each path has a power of $1/P$. Fig. 8 shows the coded BER performance in SISO and (1×2) -AFDM systems. The main observations are summarized as follows: 1) AFDM achieves a BER performance similar to that of OFDM systems when a conventional MMSE-LDPC receiver is applied. This is reasonable as coded OFDM can also exploit multipath diversity, as pointed out in [8];

2) The proposed receivers achieve about 2 dB gain over the MMSE-LDPC receiver, where the gain is more prominent as P and N_r increase. This indicates that the proposed receivers can better exploit the diversity gain of MIMO-AFDM systems than the MMSE-LDPC receiver. In addition, the proposed receivers also achieve better coded BER performance than the turbo-IDD receivers; 3) It is interesting to observe that the BP-JSG achieves a similar BER performance to EP-JSG. In addition, the proposed E-JSG has a slightly performance degradation

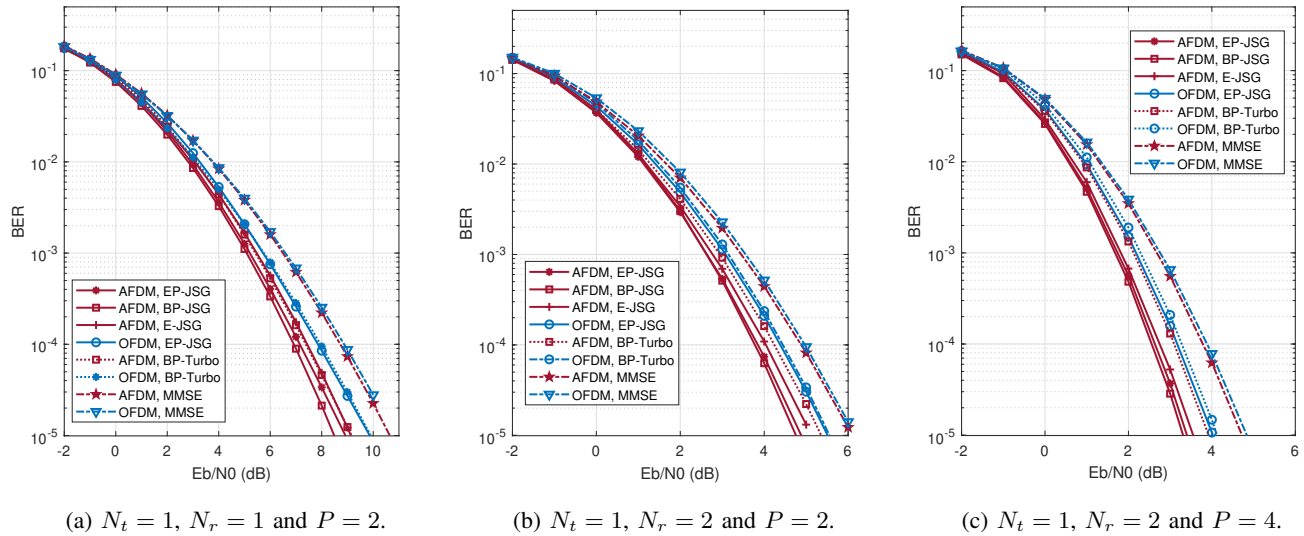


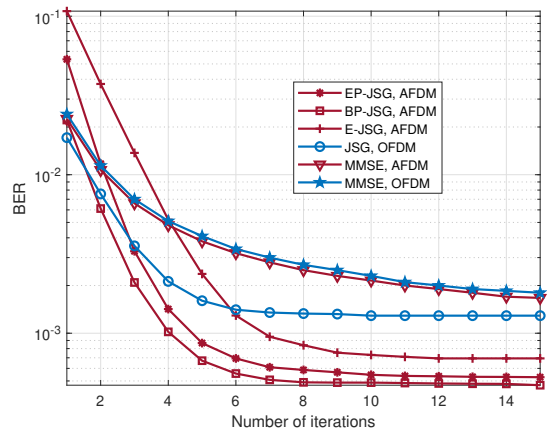
Fig. 8: Coded BER performance comparisons of different receivers.

compared to that of the EP-JSG, where the gap becomes negligible as P and N_r increase. Similar observations have also been reported in sparse code multiple access systems with turbo-like receivers [42]. This indicates that using both $\text{KL}(p|q)$ and $\text{KL}(q|p)$ in the proposed JSG can well approximate the *a posteriori* probability of \mathbf{x} .

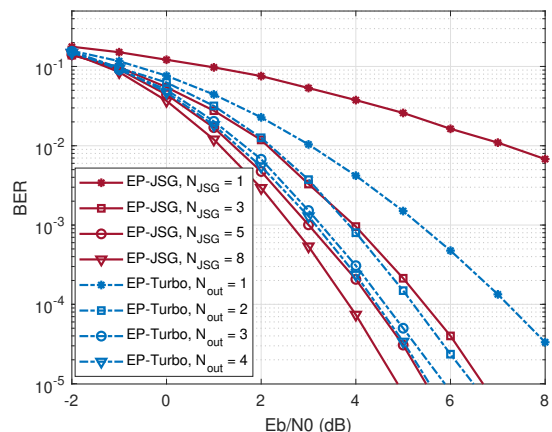
Fig. 9a shows the BER performance with different number of iterations for various receivers in the MIMO-AFDM settings of $N_t = 1, N_r = 2$ and $P = 2$. As can be seen from the figure, the proposed BP-JSG and EP-JSG need about 7 iterations to converge, whereas about 9 and 11 iterations are required for the proposed E-JSG and MMSE-LDPC receivers, respectively. It should be noted that the proposed E-JSG allows a simultaneously detection and decoding at each iteration, and eliminates the need for interleavers, de-interleavers, symbol-to-bit, and bit-to-symbol LLR transformations. Fig. 9b shows the coded BER performance at different iterations for the JSG and turbo receivers. For simplicity, the EP-JSG and EP-turbo-IDD are considered. As can be seen from the figure, the EP-turbo-IDD receiver almost converges after 3 outer iterations. Namely, about 9 EP and LDPC iterations in total. Moreover, consider the same number of EP and LDPC iterations, the proposed EP-JSG achieves better BER performance. For example, the proposed EP-JSG achieves about 2 dB gain compared to that of the EP-turbo-IDD receiver at the $\text{BER} = 10^{-4}$ for 3 iterations, i.e., $N_{\text{iter}}^{\text{out}} = 1$.

Fig. 10 shows the coded BER performance in an (2×2) -AFDM system. Specifically, both transmission scenarios 1 and 2 are considered. For multiplexing transmission of Scenario 1, the MMSE-LDPC deteriorates significantly. Notably, the proposed E-JSG for the diversity and multiplexing transmissions achieve about 2 dB and 4 dB gains, respectively, compared to the MMSE-LDPC receivers for $P = 2$. In addition, compared to the (1×2) MIMO setting in Fig. 8, the performance of (2×2) -AFDM with diversity transmission shows no improvement. This occurs because the transmit antennas may share the same delay taps, leading to a sacrifice in diversity.

Next, we present the coded BER performance and compu-



(a) BER v.s. Number of iterations.

(b) BER v.s. number of iterations ($P = 2$).Fig. 9: Convergence behavior comparisons of different receivers for (1×2) MIMO setting.

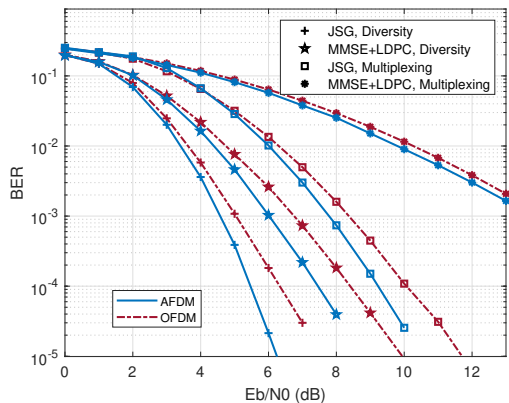
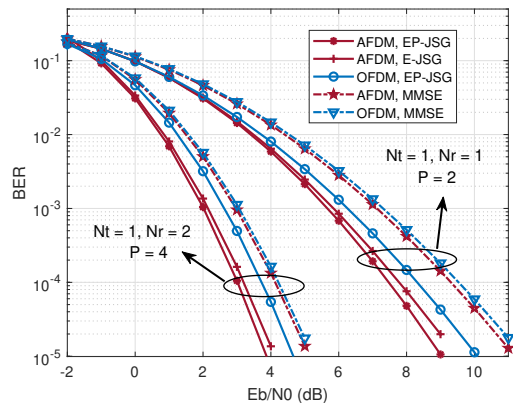
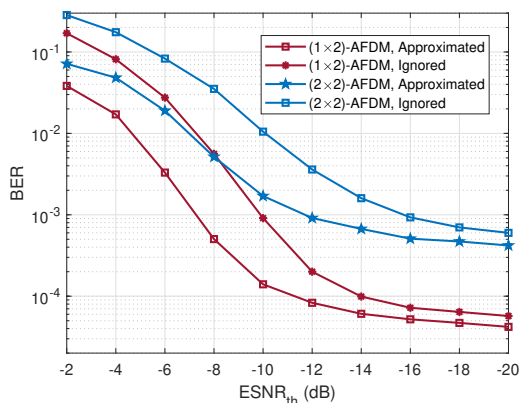
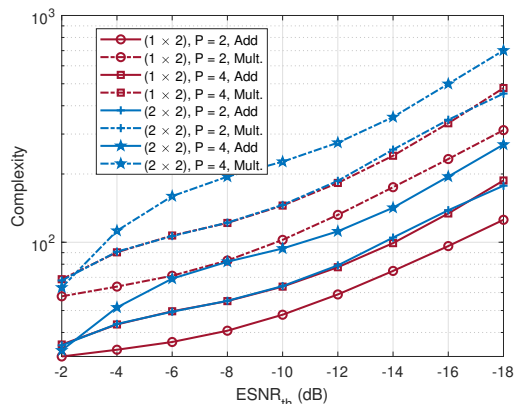
Fig. 10: BER performance of (2×2) -AFDM systems.

Fig. 12: BER performance with Doppler effects.

(a) BER performance v.s. $eSNR_{th}$ ($P = 4$).(b) Complexity v.s. $eSNR_{th}$.Fig. 11: Coded BER performance and complexity comparisons with different $eSNR_{th}$ values.

tational complexity of the proposed sparse channel message propagation method based on $eSNR$, which is shown in Fig. 11. Fig. 11(a) illustrates the coded BER performance with different $eSNR$ thresholds. The curves labeled “Approximated” represent the proposed scheme, whereas “Ignored” indicates that the insignificant edges in $D_L(n, r)$ are ignored. Clearly, when these insignificant edges are ignored, the performance deteriorates significantly, particularly for small values of $eSNR_{th}$. It is also observed that the performance of the proposed E-JSG deteriorates rapidly for $eSNR_{th} > -12$ dB.

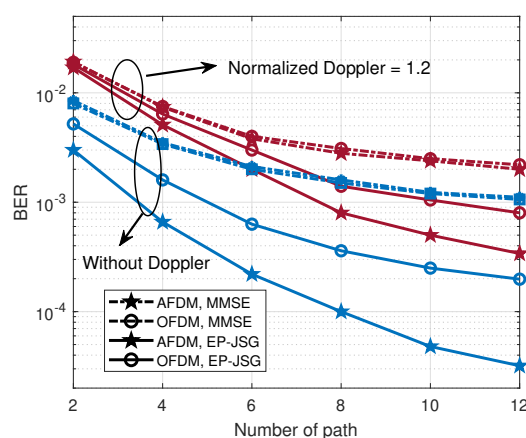
Fig. 13: Coded BER performance v.s. number of path in (1×2) -AFDM and -OFDM systems at the $E_b/N_0 = 2$ dB.

Fig. 11(b) shows the average number of addition and multiply operations of each node at each iteration for different MIMO-AFDM settings. Interestingly, the computational complexity decreases almost linearly as $eSNR_{th}$ increases. This indicates that as $eSNR_{th}$ increases, the average d_f and d_v at each FN and VN also decrease linearly. Consider the trade-off between BER performance and computational complexity, we set $eSNR_{th} = -12$ dB for both JSG and E-JSG.

Fig. 12 shows the coded BER performance of MIMO-AFDM in a fast time-varying channel with the maximum normalized Doppler $\nu_{max} = 0.075$ and $eSNR_{th} = -12$ dB. The proposed E-JSG and MMSE-LDPC receivers are considered as benchmarks for comparison. The normalized Doppler shift at the p th path is given by $\nu_p = \nu_{max} \cos(\psi_p)$ where ψ_p has a uniform distribution of $\psi_{p,i} \sim \mathcal{U}[-\pi, \pi]$. The proposed sparse channel scheme is applied to both JSG and E-JSG. As observed from the figure, the proposed E-JSG receiver exhibits approximately a 2 dB improvement over the MMSE-LDPC receiver at the BER of 10^{-5} for SISO-AFDM with $P = 2$. For the (2×2) -AFDM with $P = 4$, the gain is approximately 1 dB. Additionally, there is a performance degradation of about 0.7 dB for the proposed receiver compared to the MIMO-AFDM with zero Doppler.

Fig. 13 further demonstrates the coded BER performance in OFDM and AFDM systems as the number of paths increases

by considering a high-mobility channel with severe Doppler effect, i.e., $\nu_{\max} = 1.2$. Specifically, we consider the MMSE and EP-JSG receivers, and a (1×2) MIMO setting. We assume each path has the same power, and N_{cnp} is larger than the maximum integer delay. Both AFDM and OFDM with MMSE and EP-JSG perform better as P increases, indicating that AFDM and OFDM with MMSE and EP-JSG receivers are able to collect the diversity gain even in the presence of severe Doppler effect ($\nu_{\max} = 1.2$). Moreover, the gap between AFDM and OFDM with the proposed EP-JSG becomes smaller for $\nu_{\max} = 1.2$ compared to the case with no Doppler. This is reasonable, as more channel elements in the AFDM system are approximated by the proposed sparse channel scheme for $\nu_{\max} = 1.2$ compared to the case of $\nu_{\max} = 0$. However, AFDM with the proposed JSG receiver still achieves better BER performance than OFDM systems or MMSE receivers.

VI. CONCLUSION

In this paper, we have proposed JSG receivers for MIMO-AFDM systems. Specifically, the BP and EP as detection techniques have been introduced based on a unified VI perspective. In addition, by representing the VI graph and the LDPC codes as bipartite graphs, we have constructed a JSG for MIMO-AFDM, which enables simultaneous detection and decoding. We delve into the detailed messaging propagation over the proposed JSG. In addition, we have further proposed an E-JSG receiver based on a linear constellation encoding model, which can eliminate the need for interleavers, de-interleavers, and LLR transformations, thereby enhancing detection and decoding efficiency. Additionally, we have introduced a sparse channel method to reduce detection complexity. Simulation results demonstrated the superiority of our approach, in terms of computational complexity, latency, and error rate performance over conventional receivers. We have showed that the proposed JSG receivers efficiently exploit multipath and Doppler diversity, thereby outperforming conventional MMSE and turbo-IDD receivers, and demonstrating the superiority of AFDM over OFDM.

REFERENCES

- [1] M. Giordani, M. Polese, M. Mezzavilla, S. Rangan, and M. Zorzi, "Toward 6G networks: Use cases and technologies," *IEEE Commun. Mag.*, vol. 58, no. 3, pp. 55–61, 2020.
- [2] M. Noor-A-Rahim, Z. Liu, H. Lee, M. O. Khyam, J. He, D. Pesch, K. Moessner, W. Saad, and H. V. Poor, "6G for vehicle-to-everything (V2X) communications: Enabling technologies, challenges, and opportunities," *Proceedings of the IEEE*, vol. 110, no. 6, pp. 712–734, 2022.
- [3] S. Li, J. Yuan, W. Yuan, Z. Wei, B. Bai, and D. W. K. Ng, "Performance analysis of coded OTFS systems over high-mobility channels," *IEEE Trans. Wireless Commun.*, vol. 20, no. 9, pp. 6033–6048, 2021.
- [4] Y. Zhou, H. Yin, J. Xiong, S. Song, J. Zhu, J. Du, H. Chen, and Y. Tang, "Overview and performance analysis of various waveforms in high mobility scenarios," in *2024 ICCET*, 2024, pp. 35–40.
- [5] G. Stuber, J. Barry, S. McLaughlin, Y. Li, M. Ingram, and T. Pratt, "Broadband MIMO-OFDM wireless communications," *Pro. IEEE*, vol. 92, no. 2, pp. 271–294, 2004.
- [6] P. Raviteja, Y. Hong, E. Viterbo, and E. Biglieri, "Effective diversity of OTFS modulation," *IEEE Wireless Commun. Lett.*, vol. 9, no. 2, pp. 249–253, 2020.
- [7] X. Ouyang and J. Zhao, "Orthogonal chirp division multiplexing," *IEEE Trans. Commun.*, vol. 64, no. 9, pp. 3946–3957, 2016.
- [8] M. S. Omar and X. Ma, "Performance analysis of OCDM for wireless commun." *IEEE Trans. Wireless Commun.*, vol. 20, no. 7, pp. 4032–4043, 2021.
- [9] W. Yuan, Z. Wei, J. Yuan, and D. W. K. Ng, "A simple variational Bayes detector for orthogonal time frequency space (OTFS) modulation," *IEEE Trans. Veh. Technol.*, vol. 69, no. 7, pp. 7976–7980, July 2020.
- [10] H. Haif, S. E. Zegrar, and H. Arslan, "Novel OCDM transceiver design for doubly-dispersive channels," *IEEE Trans. Veh. Technol.*, pp. 1–11, 2024.
- [11] A. Bemani, N. Ksairi, and M. Kountouris, "Affine frequency division multiplexing for next generation wireless communications," *IEEE Trans. Wireless Commun.*, vol. 22, no. 11, pp. 8214–8229, 2023.
- [12] T. Erseghe, N. Laurenti, and V. Cellini, "A multicarrier architecture based upon the affine Fourier transform," *IEEE Trans. Commun.*, vol. 53, no. 5, pp. 853–862, May 2005.
- [13] A. Bemani, G. Cuzzo, N. Ksairi, and M. Kountouris, "Affine frequency division multiplexing for next-generation wireless networks," in *2021 17th ISWCS*, 2021, pp. 1–6.
- [14] Y. Ni, Z. Wang, P. Yuan, and Q. Huang, "An AFDM-based integrated sensing and communications," in *ISWCS*, Hangzhou, China, 2022, pp. 1–6.
- [15] V. Savaux, "DFT-based modulation and demodulation for affine frequency division multiplexing," Aug. 2023. [Online]. Available: https://www.techrxiv.org/articles/preprint/DFT-Based_Modulation_and_Demodulation_for_Affine_Frequency_Division_Multiplexing/23804055
- [16] Y. Tang, A. Zhang, M. Wen, Y. Huang, F. Ji, and J. Wen, "Time and frequency offset estimation and intercarrier interference cancellation for AFDM systems," in *2024 IEEE WCNC*, 2024, pp. 1–6.
- [17] H. Yin and Y. Tang, "Pilot aided channel estimation for AFDM in doubly dispersive channels," in *2022 IEEE ICC*, 2022, pp. 308–313.
- [18] H. Yin, X. Wei, Y. Tang, and K. Yang, "Diagonally reconstructed channel estimation for MIMO-AFDM with inter-Doppler interference in doubly selective channels," *IEEE Trans. Wireless Commun.*, pp. 1–1, June, 2024.
- [19] A. Bemani, N. Ksairi, and M. Kountouris, "Low complexity equalization for AFDM in doubly dispersive channels," in *2022 IEEE ICASSP*, 2022, pp. 5273–5277.
- [20] L. Wu, S. Luo, D. Song, F. Yang, and R. Lin, "A message passing detection based affine frequency division multiplexing communication system," Aug. 2023. [Online]. Available: <https://arxiv.org/abs/2307.16109>
- [21] J. Zhu, Y. Tang, X. Wei, H. Yin, J. Du, Z. Wang, and Y. Liu, "A low-complexity radar system based on affine frequency division multiplexing modulation," 2023. [Online]. Available: <https://arxiv.org/abs/2312.11125>
- [22] Y. Ni, Z. Wang, P. Yuan, and Q. Huang, "An AFDM-based integrated sensing and communications," in *2022 ISWCS*. IEEE, 2022, pp. 1–6.
- [23] A. Bemani, N. Ksairi, and M. Kountouris, "Integrated sensing and communications with affine frequency division multiplexing," *IEEE Wireless Commun. Lett.*, vol. 13, no. 5, pp. 1255–1259, 2024.
- [24] Q. Luo, P. Xiao, Z. Liu, Z. Wan, N. Thomos, Z. Gao, and Z. He, "AFDM-SCMA: A promising waveform for massive connectivity over high mobility channels," *IEEE Trans. Wireless Commun.*, vol. Early Access, 2024.
- [25] Y. Tao, M. Wen, Y. Ge, and J. Li, "Affine frequency division multiplexing with index modulation," in *2024 IEEE WCNC*, 2024, pp. 1–6.
- [26] J. Zhu, Q. Luo, G. Chen, P. Xiao, and L. Xiao, "Design and performance analysis of index modulation empowered AFDM system," *IEEE wireless commun. lett.*, 2023.
- [27] Q. Luo, J. Zhu, P. Xiao, G. Chen, J. Shi, and C. Lu, "Building MIMO-SCMA upon affine frequency division multiplexing for massive connectivity over high mobility channels," in *2024 IEEE VTC2024-Spring*, 2024, pp. 1–6.
- [28] X. Ma and G. Giannakis, "Maximum-diversity transmissions over doubly selective wireless channels," *IEEE Tran. Inf. Theory*, vol. 49, no. 7, pp. 1832–1840, 2003.
- [29] Q. Luo, Z. Liu, G. Chen, and P. Xiao, "Enhancing signal space diversity for SCMA over Rayleigh fading channels," *IEEE Trans. Wireless Commun.*, vol. 23, no. 4, pp. 3676–3690, 2024.
- [30] L. Hanzo, J. P. Woodard, and P. Robertson, "Turbo decoding and detection for wireless applications," *Proceedings of the IEEE*, vol. 95, no. 6, pp. 1178–1200, 2007.
- [31] L. Liu, S. Liang, and L. Ping, "On capacity optimality of OAMP: Beyond IID sensing matrices and gaussian signaling," *IEEE Trans. Commun.*, 2024.
- [32] L. Zhao, W.-J. Gao, and W. Guo, "Sparse Bayesian learning of delay-Doppler channel for OTFS system," *IEEE Commun. Lett.*, vol. 24, no. 12, pp. 2766–2769, 2020.

- [33] C. Zhang, J. Bütepage, H. Kjellström, and S. Mandt, “Advances in variational inference,” *IEEE Trans. Pattern Anal. Mach. Intell.*, vol. 41, no. 8, pp. 2008–2026, 2019.
- [34] X. Meng, L. Zhang, C. Wang, L. Wang, Y. Wu, Y. Chen, and W. Wang, “Advanced NOMA receivers from a unified variational inference perspective,” *IEEE J. Sel. Areas Commun.*, vol. 39, no. 4, pp. 934–948, 2021.
- [35] W. Yuan, Z. Wei, J. Yuan, and D. W. K. Ng, “A simple variational bayes detector for orthogonal time frequency space (OTFS) modulation,” *IEEE Trans. Veh. Tech.*, vol. 69, no. 7, pp. 7976–7980, 2020.
- [36] L. Wen, R. Razavi, M. A. Imran, and P. Xiao, “Design of joint sparse graph for OFDM system,” *IEEE Trans. Wireless Commun.*, vol. 14, no. 4, pp. 1823–1836, 2015.
- [37] F. Kschischang, B. Frey, and H.-A. Loeliger, “Factor graphs and the sum-product algorithm,” *IEEE Trans. Inf. Theory*, vol. 47, no. 2, pp. 498–519, 2001.
- [38] X. Meng, S. Wu, L. Kuang, and J. Lu, “An expectation propagation perspective on approximate message passing,” *IEEE Signal Process. Lett.*, vol. 22, no. 8, pp. 1194–1197, 2015.
- [39] T. P. Minka, “Expectation propagation for approximate bayesian inference,” Jul. 2013. [Online]. Available: <https://arxiv.org/abs/1301.2294>
- [40] Q. Luo, Z. Liu, G. Chen, Y. Ma, and P. Xiao, “A novel multitask learning empowered codebook design for downlink SCMA networks,” *IEEE Wireless Commun. Lett.*, vol. 11, no. 6, pp. 1268–1272, 2022.
- [41] 3GPP, “5G NR; multiplexing and channel coding.” [Online]. Available: <https://portal.3gpp.org/desktopmodules/Specifications/SpecificationDetails.aspx?specificationId=3214>
- [42] W. Yuan, N. Wu, Q. Guo, Y. Li, C. Xing, and J. Kuang, “Iterative receivers for downlink MIMO-SCMA: Message passing and distributed cooperative detection,” *IEEE Trans. Wireless Commun.*, vol. 17, no. 5, pp. 3444–3458, 2018.